Neural Activity in Superior Parietal Cortex during Rule-based Visual-motor Transformations

Kara M. Hawkins, Patricia Sayegh, Xiaogang Yan, J. Douglas Crawford, and Lauren E. Sergio

Abstract

■ Cognition allows for the use of different rule-based sensorimotor strategies, but the neural underpinnings of such strategies are poorly understood. The purpose of this study was to compare neural activity in the superior parietal lobule during a standard (direct interaction) reaching task, with two nonstandard (gaze and reach spatially incongruent) reaching tasks requiring the integration of rule-based information. Specifically, these nonstandard tasks involved dissociating the planes of reach and vision or rotating visual feedback by 180°. Single unit activity, gaze, and reach trajectories were recorded from two female *Macaca mulattas*. In all three conditions, we observed a temporal discharge pattern at the population level reflecting early reach planning and on-line reach monitoring. In the plane-dissociated task, we found a significant overall attenuation in the discharge rate of cells from deep recording sites, relative to standard reaching. We also found that cells modulated by reach direction tended to be significantly tuned either during the standard or the plane-dissociated task but rarely during both. In the standard versus feedback reversal comparison, we observed some cells that shifted their preferred direction by 180° between conditions, reflecting maintenance of directional tuning with respect to the reach goal. Our findings suggest that the superior parietal lobule plays an important role in processing information about the nonstandard nature of a task, which, through reciprocal connections with precentral motor areas, contributes to the accurate transformation of incongruent sensory inputs into an appropriate motor output. Such processing is crucial for the integration of rule-based information into a motor act. ■

INTRODUCTION

Cognition allows one to flexibly engage various learned rules for sensorimotor integration (Bunge et al., 2005; White & Wise, 1999). To date there has been a great deal of research on both the neurophysiology of motor control and the neural activity associated with cognitive rule processing. However, there has been relatively little research on the neurophysiology of cognitive-motor integration, where rules dictate the relationship between perception and action (Georgopoulos, 2000). Instead, most previous studies of visuomotor physiology have focused on the issue of how interconnected neuronal populations from parietal, premotor, and primary motor areas may perform transformations from extrinsic spatial representations to intrinsic joint and muscle representations (Crawford, Henriques, & Medendorp, 2011; Sergio & Kalaska, 2003; Battaglia-Mayer et al., 2000; Colby & Goldberg, 1999; Kalaska, Sergio, & Cisek, 1998; Shen & Alexander, 1997; Zhang, Riehle, Requin, & Kornblum, 1997; Johnson, Ferraina, Bianchi, & Caminiti, 1996; Crutcher & Alexander, 1990; Flash & Mussa-Ivaldi, 1990). The purpose of the current study was to understand how neural activity in the parietal component of these pathways is altered when monkeys are trained to integrate different visual-motor rules into their reaching behavior.

Much of our reaching behavior involves directly interacting with the object that we are viewing. Visuomotor transformations such as these can be considered "standard" because the visual stimulus guiding the action is itself the target of the action. However, the evolution of the capacity for tool use in primates has resulted in situations where the correspondence between vision and action is not direct. Rather, the mapping between stimulus and response must be learned and calibrated (Sergio, Gorbet, Tippett, Yan, & Neagu, 2009; Bo, Contreras-Vidal, Kagererm, & Clark, 2006; Piaget, 1965). A common example is the use of a computer mouse: You push the mouse forward on a horizontal table to displace a cursor upward on a vertical monitor. A less common example is laparoscopic surgery, where the surgeon must manipulate instruments, often levered, while viewing the surgical field on a monitor away from the actual body being operated on. This type of situation has been referred to as "nonstandard" sensorimotor mapping (Wise, di Pellegrino, & Boussaoud, 1996). In nonstandard visually guided reaching, the visual information used to perform the reach does not necessarily come from the object that one's hand is interacting with. Thus, such nonstandard tasks require the incorporation

York University, Toronto, Canada

of spatial or cognitive rules into the movement for successful performance.

In everyday life, we perform nonstandard reaches routinely. A large amount of evidence suggests that movements of the eyes and hands are tightly coupled (Neggers & Bekkering, 2000; Henriques, Klier, Smith, Lowy, & Crawford, 1998; Sergio & Scott, 1998; Vercher, Magenes, Prablanc, & Gauthier, 1994; Gauthier & Mussa-Ivaldi, 1988; Gielen, Van Den Heuvel, & Van Gisbergen, 1984; Morasso, 1981; Prablanc, Echallier, Komilis, & Jeannerod, 1979), which makes sense from an evolutionary perspective (i.e., many of our behaviors involve acting directly on visually perceived objects in the environment). What remains unclear, however, is how this natural eye–hand coupling is inhibited to learn and perform movements that involve dissociating the eyes from the hand (Gorbet & Sergio, 2009). Previous research has indicated that activity in the parietal-frontal reach network is altered between standard and nonstandard reaches and that different parieto-frontal pathways may be involved in integrating cognition with action (Gorbet & Sergio, 2007; Gorbet, Staines, & Sergio, 2004). Furthermore, it has been shown that the ability to perform nonstandard reaches can deteriorate under neuropathological conditions such as Alzheimer's disease (Tippett & Sergio, 2006; Ghilardi et al., 1999) and mild cognitive impairment (Salek, Anderson, & Sergio, 2011). There is some evidence that this behavioral decline may be related to hypometabolism in the parietal cortex and/or deterioration in communication between parietal and precentral motor areas (Jacobs et al., 2010; Schroeter, Stein, Maslowski, & Neumann, 2009; Tippett, Krajewski, & Sergio, 2007; Braak & Braak, 1991). To date, however, parietal activity at a single cell or cell assembly level specifically examining standard versus nonstandard reaching has not been characterized.

The aim of the current study was to examine neural activity in the superior parietal lobule (SPL) during nonstandard reaching. Our hypotheses were tested on a single cell level by maintaining reach behavior constant while manipulating visual feedback, thereby altering the level of visuomotor congruence. Our first hypothesis was that the output from cells within the SPL would be diminished during nonstandard visuomotor transformations, reflecting inhibition of the natural tendency to interact directly with visually acquired targets (Gorbet et al., 2004; Neggers & Bekkering, 2000; Gielen et al., 1984). From this hypothesis, we predicted that multimodal SPL cells would display reduced cell activity and that fewer cells would demonstrate directional tuning when gaze and hand locations were incongruent. Our second hypothesis was that cell activity in this area, given strong proprioceptive inputs and efferent connections to more caudal dorsal premotor areas, would reflect the motor goal of the task rather than the visual goal when the two are decoupled (Gail, Klaes, & Westendorff, 2009; Redding, Rossetti, & Wallace, 2005; Johnson et al., 1996; Kalaska, 1996; Redding & Wallace, 1996). From this hypothesis, we predicted that cells would alter their directional tuning to follow the new movement goal during a visual feedback reversal task (180° away from the visual target).

Here we demonstrate that neurons from deep SPL recording sites show modulation early in the planning period across tasks (Gamberini et al., 2009; Prado et al., 2005; Galletti, Fattori, Kutz, & Gamberini, 1999). We also observe resurgence in activity during movement, which may reflect the on-line monitoring of reach execution (Archambault, Ferrari-Toniolo, & Battaglia-Mayer, 2011; Archambault, Caminiti, & Battaglia-Mayer, 2009; Desmurget et al., 1999). Importantly, we find that both mean cell discharge rates and directional tuning change as a function of task. These data support our hypothesis that this brain region is involved in the cognitive-motor integration required for nonstandard rule-based action.

METHODS

Subjects

Two monkeys (*Macaca mulatta*, females, G and B, 5.4/5.2 kg, respectively) were trained to perform motor control tasks using a visually instructed center-out delayed reaching paradigm, monkey G with the left hand and monkey B with the right hand. Recordings were made from the contralateral hemisphere. All surgical and animal handling procedures were in accordance with Canadian Council on Animal Care guidelines on the use of laboratory animals and preapproved by the York University Animal Care Committee.

Behavioral Setup and Protocol

During task performance, the monkey was seated in a primate chair positioning its eyes 40 cm from a 15-in. vertically positioned standard monitor, which was set at eye level and centered with its midline. The animal's head was restrained by a head post, and its arm was positioned over a 15-in. horizontal touch-sensitive monitor placed 40 cm from the animal's eyes and set between its waist and xyphoid process, allowing comfortable reaching over the entire surface. A small lever was positioned at the bottom of the touch monitor to provide a resting place for the nonreaching arm and ensure that it remained off the touch monitor during the experiment.

Monkey G learned to perform standard and plane dissociated reaching, and monkey B learned to perform standard, plane dissociated, and feedback reversal reaching. At the beginning of each trial for all three conditions, a red circular target (70 mm in diameter; 10° of visual angle) with an inner white colored circle (40 mm in diameter; 5.7° of visual angle) appeared on the screen. The red target instructed where the monkey was required to touch and the white circle instructed where the monkey was required to fixate. After holding the center target for

500 msec (preCUE), one of eight green-colored peripheral targets (70 mm in diameter; 10° of visual angle, with an inner 40 mm/5.7° white eye tolerance circle) appeared (distance between the midpoint of the central target and the midpoint of the peripheral targets was 80 mm, subtending 11.4° of visual angle). All eight peripheral targets were equally spaced around the central target, with 45° between them (0° through 315°, 0° to the right). After a variable delay period of 2000 ± 500 msec (CUE) the central target extinguished, serving as a go signal for the monkey to look and reach toward the peripheral target by sliding its hand along the touch monitor. The CUE period was further divided into an early portion (onset of peripheral target plus 600 msec: eCUE) and a late portion (offset of central target minus 600 msec: lCUE). The RT epoch was the interval between the go signal and the monkey's initial hand movement (i.e., movement onset), judged as 8% peak velocity. RTs less than 150 msec and greater than 800 msec were considered erroneous, resulting in termination of the trial. The movement time (MT) epoch was the time period between movement onset and movement offset, judged as 8% peak velocity along with arrival at the peripheral target. An MT of more than 800 msec was considered erroneous, resulting in trial termination. Once the eyes and the hand arrived at the appropriate target location, the monkey was required to hold both its eyes and hand in place for a target hold (TH) period of 500 msec to obtain a liquid reward (Figure 1A).

Presentation of the eight peripheral targets was repeated five times in a randomized-block design, so that each block consisted of 40 trials. The monkey completed a block of 40 trials in one condition before performing a block in one of the other conditions. The order in which each condition was presented varied from day to day, and duplicate sets of block data files were occasionally collected from the same cell to ensure reproducibility of results. For all conditions, the room lighting was kept dim, but not completely dark.

In the standard condition, the visual targets were presented on the horizontal touch screen and the animal was required to move its eyes and slide its hand to the illuminated peripheral target upon receiving the go signal. In other words, this condition required acquiring the target with both the eyes and the hand in a spatially congruent fashion. In the plane dissociation condition, the monkey's hand movements remained on the horizontal screen; however, the direction of the required reach was indicated by a visual target presented on the vertical screen. In other words, this task required the animal to direct its eyes and move a cursor (crosshair) toward a target on the vertical screen by sliding its hand on the horizontal screen. Thus, the target acquired by the eyes was not spatially congruent with that acquired by the hand. An opaque board was placed 10 cm above the animal's arm to block vision of the hand. Importantly, the required reaching movements in this condition were identical to those in the standard condition. In the feedback reversal condition, the visual targets were presented on the horizontal screen, as in the standard condition, however the animal was required to look toward the target while sliding its hand in the

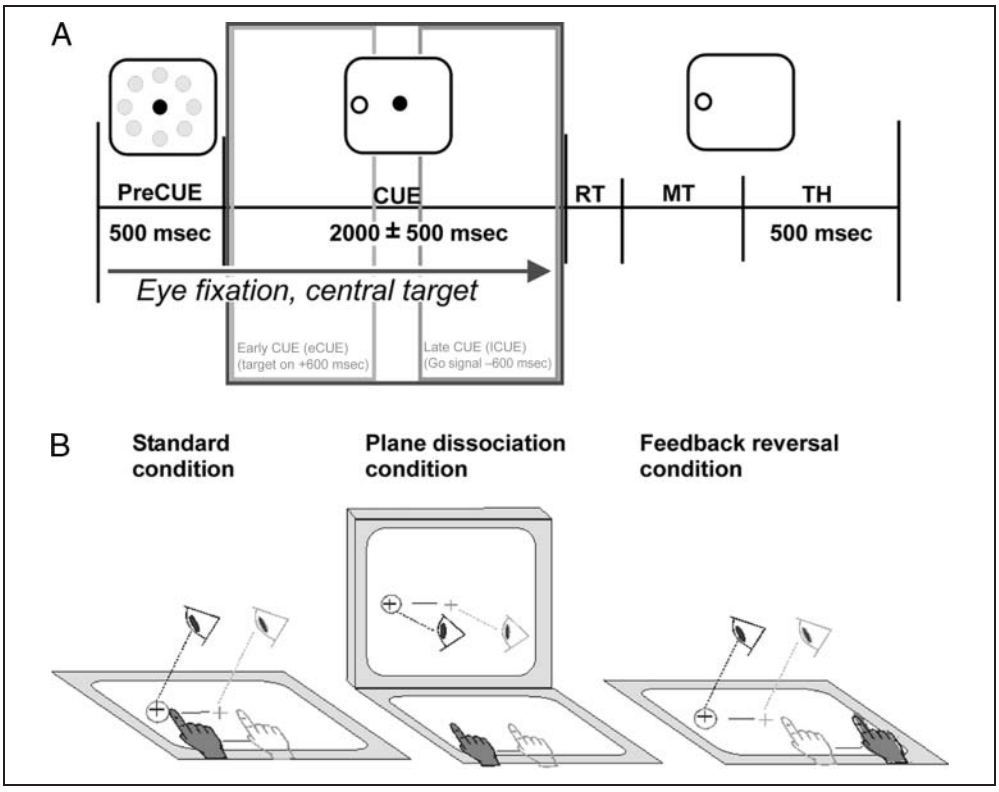

Figure 1. Trial timing and experimental setup. (A) In each trial, one of eight equally spaced (45°) peripheral targets was presented on either a touch-sensitive screen placed over the animal's lap or on a monitor positioned vertically 40 cm from the animal's frontal plane. Arm movements were always made over the horizontal touch screen. Light gray circles represent the eight target locations (not actually illuminated during preCUE). Open circles represent the green-colored peripheral target; black circles represent the red-colored central target. (B) Schematic drawings of the standard, plane dissociation, and feedback reversal conditions. The animal's head was fixed throughout the experiment.

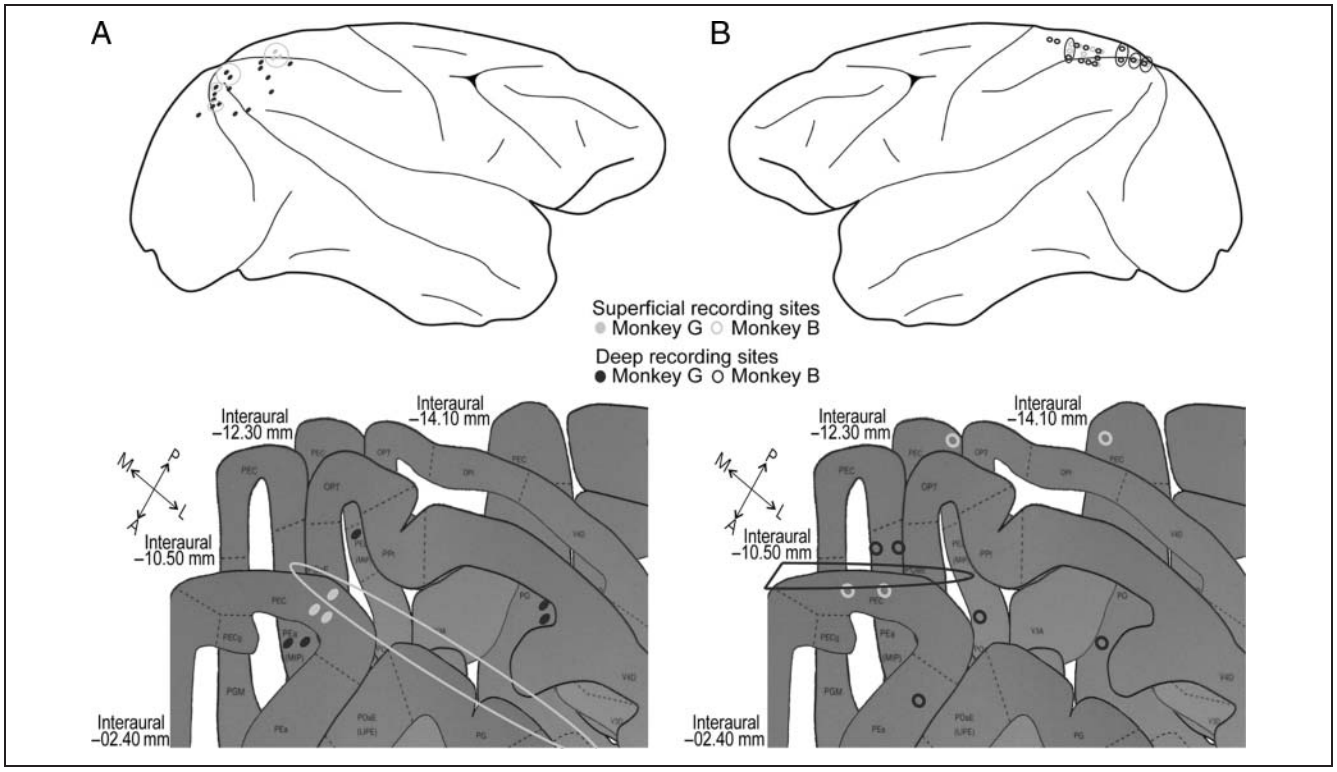

Figure 2. Reconstruction of recording penetrations. (A) Monkey G (right hemisphere): Recording sites were restricted to the medial-anterior portion of the recording chamber providing access to the anterior walls of the intraparietal and parietal-occipital sulci through deep electrode penetrations (solid black circles). Some superficial sites (area PEc) were also accessible at the medial edge of the chamber (solid gray circles). (B) Monkey B (left hemisphere): Half of the recording chamber (centered on the longitudinal fissure) was opened providing access to area PEc through superficial penetrations (open gray circles), and the intraparietal and parietal-occipital sulci through deep penetrations in the anterior and posterior portions of the chamber, respectively (open black circles). Bottom: selected penetration sites from both animals (circled, top) displayed on coronal slices. Gray oval represents recording chamber placement for monkey G; black semioval represents recording chamber placement for monkey B.

opposite direction to guide the cursor toward the target. Thus, reaches performed in this condition were identical to those in the other two conditions, but with visual feedback rotated 180° from the hand. No cue was used to signal the feedback reversal task, but rather the animal learned through trial and error which movement direction would result in a reward at the beginning of the condition block, after which she was able to continue with the appropriate task (Figure 1B).

Surgical Procedures

Surgeries were performed after the animals had been trained to achieve >60% success rates on all tasks. In both animals, implantation of the recording chamber (19 mm internal diameter) over the SPL was performed using standard aseptic surgical techniques (Kalaska, Cohen, Hyde, & Prud'homme, 1989). The stereotaxic coordinates for monkey G (interaural; A: −12.30 mm, L: 18.40 mm) were selected to provide access to cortical regions within the parietal-occipital sulcus (POs) and the intraparietal sulcus (IPS). Space limitations, due to a previously implanted premotor chamber and a posterior head-post, did not allow for direct placement over the cortical areas of interest for monkey G. This resulted in positioning the chamber on a 25° angle to allow access to the desired brain regions through deep electrode penetrations in the medial-anterior quadrant of the chamber (Figure 2A). The stereotaxic coordinates for monkey B (interaural; A: −7.80 mm, L: 00.00 mm) were selected to provide access to both the right and left hemispheres (recordings in the current study were from the left hemisphere only), spanning over PEc, IPS, and POs (Figure 2B). The experiments began 7–10 days after surgery following a complete recovery.

Neural and Behavioral Recordings

A multichannel hydraulic driver (MCM-4, FHC, Inc., Bowdoin, ME), mounted on the implanted chamber, was used to advance tungsten microelectrodes into the cortex (diameter, 2–5 μm at the tip, FHC, Inc., Bowdoin, ME). These microelectrodes, in conjunction with a multichannel amplification and filtering system (MCP, Alpha-Omega Engineering, Israel), were used to receive electrical potentials from the brain. The hydraulic driver controlled each electrode separately, allowing one electrode to be advanced until it touched the dura, serving as a ground with which to compare electrical activity recorded by the electrodes descended into the cortex. One or two electrodes were advanced into the cortex at a rate of 100 μm/min while

listening for spiking activity using an auditory guidance system and monitoring for action potential waveforms using a multispike detection system (Alpha-Omega Engineering, Israel). Action potentials that showed increased activity in response to the animal reaching toward a moving screensaver, but not from visual tracking alone, were isolated and are referred to from this point on as task-related cells. A record of the depth at which each recording was made (in μm past dura) was kept. Electrical activity was amplified and band-pass filtered (100–10,000 Hz) before passing through the multispike detector. Spikes were sampled at 12.5 kHz and sorted using template matching software, which allowed up to three waveforms per electrode to be isolated. Spikes were collected in conjunction with eye and behavioral event data using an Alpha-Map data acquisition system (Alpha-Omega Engineering, Israel). Alpha-Map files were saved and converted into MATLAB format for analysis of the relationship between spiking activity and behavior.

Hand location and movements were monitored using a touch sensitive monitor capable of detecting spatial displacements as small as 3 mm using infrared beams (100 Hz, Touch Controls, Inc., San Diego, CA). The monkeys were required to maintain contact with the screen for the duration of the trial. If the animals lifted their hand for any reason, the trial would stop and another one would begin. Movement alleys were included in the touch screen program to ensure that reaches were directed along a fairly straight trajectory toward the appropriate spatial target. These alleys were set at ±40 mm from a straight line spanning from the central to the peripheral targets. If the monkey's hand deviated beyond the set alley, the trial would stop.

Eye movements were monitored using an ISCAN-ETL 200 corneal reflection eye tracking system (ISCAN, Inc., Burlington, MA) at a sampling rate of 60 Hz. The system was calibrated before running a block of trials to compute gaze intersection on either the vertical or the horizontal monitor, depending on the condition. Calibration consisted of nine targets (20 mm in diameter; 2.9° of visual angle) located in the same locations as the central and peripheral targets used during the task.

Muscle activity was recorded in monkey G from 13 proximal-arm muscles in separate recording sessions. Pairs of Teflon-insulated 50 μm single-stranded stainless steel wires were implanted percutaneously. Implantations were verified by passing current through the wires to evoke focal muscular contractions (<1.0 mA, 30 Hz, 300 msec train; Sergio & Kalaska, 2003). Multiunit EMG activity was amplified, band-pass filtered (100–3000 Hz), half-wave rectified, integrated (5 msec time bins) and digitized on-line at 200 Hz. The muscles studied included the anterior deltoid, medial deltoid, posterior deltoid, dorsoepitrochlearis, infraspinatus, latissimus dorsi, pectoralis, supraspinatus, teres major, rostral trapezius, caudal trapezius, triceps lateralis, and triceps medialis. These recordings were performed to assess the general effects of the standard and plane dissociation tasks on EMG activity and were not designed as a definitive bio-mechanical study of the muscle properties.

Behavioral Data Analysis

Reach trajectories were low-pass Butterworth filtered at 10 Hz (Matlab, Mathworks, Inc.). Movement onsets and endpoints were scored as 8% peak velocity for each trial using a custom-written program. The resultant movement trajectories were then divided into 21 equal segments and the five trials performed in each direction were pooled, allowing means and standard deviations (*SD*) to be calculated at each point along the path. An *F* ratio analysis on the trajectory standard deviations (*x* and *y* components) was performed to compare reach variability between conditions. Repeated measures ANOVAs were performed on the EMG data during the CUE and MT epochs for each muscle recorded to determine the effect of target (reach direction) and condition (standard and plane dissociation) on maximum EMG amplitude. This analysis was included to ensure that muscle activation for reach performance was the same in both conditions; thus, it was expected that reach direction would have an effect on EMG amplitude, but condition would not. Mean RTs (from the go signal to 8% peak velocity) were also calculated for each condition. Paired-sample *t* tests were performed to compare MTs and RTs between the standard and plane dissociation conditions and between the standard and feedback reversal conditions.

Neural Data Analysis

Six sequential behavioral epochs (preCUE, eCUE, lCUE, RT, MT, and TH) were defined within each trial in all three conditions (see Figure 1A). Mean neuronal discharge rates were calculated for each of the eight target directions in each condition, which allowed preferred directions (PD) to be determined (discussed below). Mean discharge rates were also calculated for each epoch (collapsed over direction) in each condition and normalized to account for variation in the baseline firing rates of individual neurons using percent dynamic range, %DR = (mean discharge/(max discharge − min discharge)) × 100. After grouping task-related cells based on depth to separate superficial (gyrus) recordings (depths < 2200 μm past dura, defined based on average gray matter thickness) from deep (sulcus) recordings (depths > 2200 μm past dura, generally 4000–8000 μm, that is, deep enough to enter the anterior wall of the IPS or POs), repeated-measures ANOVAs were performed on these separate groups of parietal cells to evaluate differences in normalized discharge rates between epochs (i.e., over time throughout the trial) and between conditions. A mixed-design ANOVA was also conducted to compare normalized mean discharge rates between recording sites in each condition. Furthermore, contrast ratios were calculated for each cell comparing grand mean discharge rates (i.e., collapsed over direction and epoch)

between conditions, (MDs − MDp)/(MDs + MDp) and (MDs − MDr)/MDs + MDr), for standard versus plane dissociation and standard versus feedback reversal conditions, respectively; where MDs represents mean discharge during the standard condition, MDp represents mean discharge during the plane dissociation condition, and MDr represents mean discharge during the feedback reversal condition. All analyses were conducted separately for standard versus plane dissociation conditions (data pooled between monkeys G and B) and standard versus feedback reversal conditions (data from monkey B only). To test for the possibility that any differences observed in mean discharge rates between the standard and plane dissociation conditions might be explained by the shift in gaze between these two tasks, we also performed a paired *t* test comparing firing rates during eye calibration on the horizontal versus vertical monitors for a random sample of deep cells (because these are the cells that exhibited modulation between the standard and plane dissociation tasks, see Results).

A custom written Matlab program was used to examine the directional tuning of cells during each trial epoch after presentation of the peripheral target (i.e., eCUE, lCUE, RT, MT, and TH). A sinusoidal regression on the mean discharge rates for each target direction was performed and the goodness of the regression fit (i.e., the proportion of total variation explained by the regression or R^2) was calculated. The regression equation was then reexpressed in terms of the peak of the sine wave, which is the direction for which the cell was most active (i.e., the "preferred direction"; Georgopoulos, Kalaska, Caminiti, & Massey, 1982). A bootstrap test was then performed using 1000 shuffled activities to determine the significance of the tuning based on a 95% confidence interval. The tuning strengths (i.e., vector lengths) of all cells exhibiting significant directional tuning were recorded, and paired *t* tests were performed comparing vector lengths between conditions. All results were considered significant at an α-level of $p < .05$.

RESULTS

Behavioral Findings

To establish the effect of task (standard, plane dissociation, and feedback reversal) on reach trajectories, an *F* ratio analysis was performed on *x* and *y* components of the 21 trajectory standard deviations computed for each movement direction (crosshairs in Figure 3, 168 points

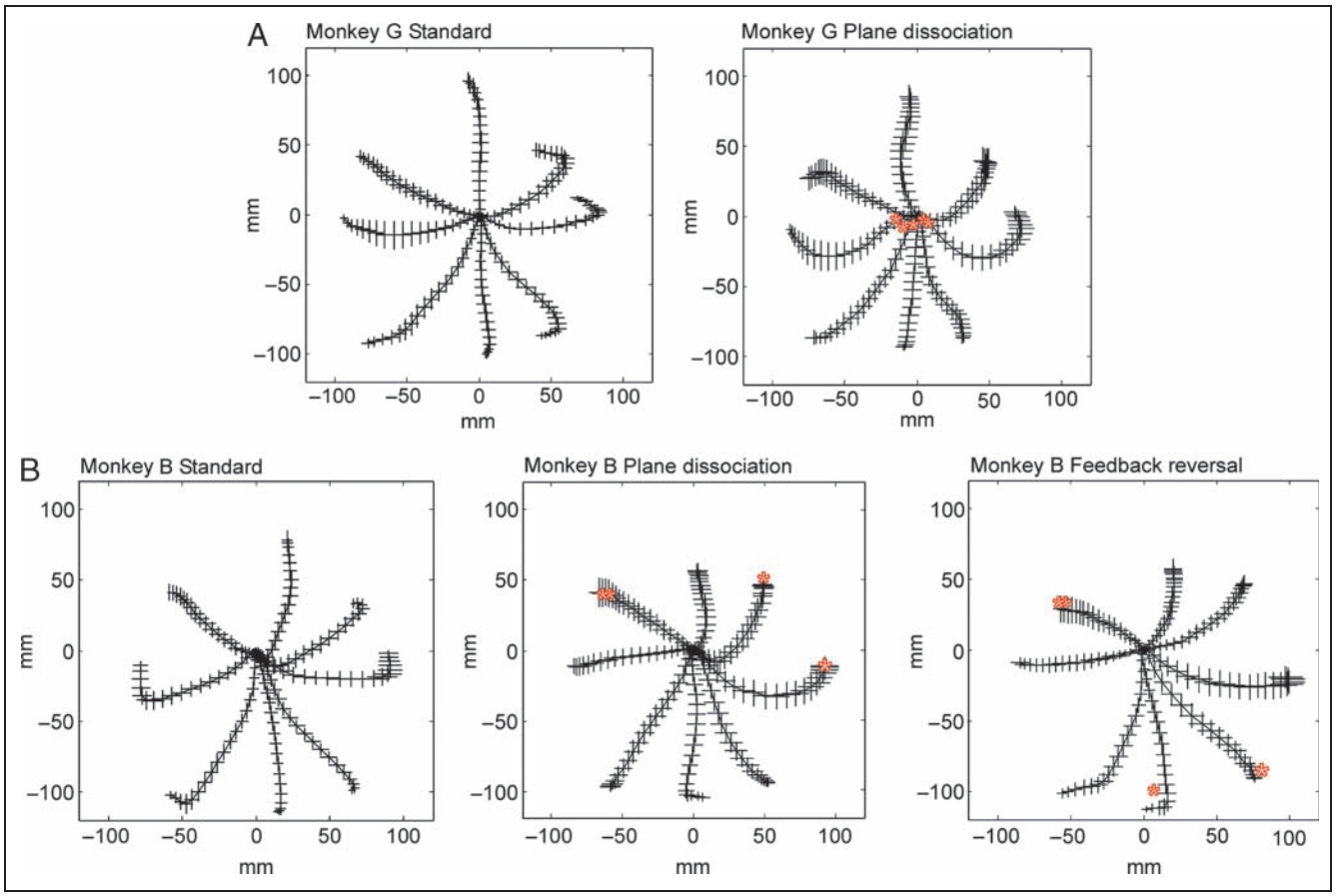

Figure 3. Mean reach trajectories. (A) Monkey G. (B) Monkey B. Center-out lines represent mean movement trajectories across recording sessions; vertical and horizontal tick marks represent standard deviations. Asterisks denote trajectory segments that were significantly ($p < .05$) more variable in comparison with the standard condition.

compared between each task condition). We observed similar variability between standard, plane dissociation, and feedback reversal conditions. There were a few points along the trajectory that showed significant differences in variability in certain directions (2.2% of points compared, $p < .05$). These differences are marked with asterisks in Figure 3 and suggest that monkey G was more variable in positioning her hand on the central target when it was not visible during the plane dissociation condition whereas monkey B exhibited an increase in endpoint variability in some reach directions during the plane dissociation and feedback reversal conditions. Over the vast majority of trajectories, however, there were no differences. With respect to muscle activity, an analysis of the EMG data revealed that for 11 of 13 muscles there was no main effect of Condition during the movement and CUE epochs ($p > .05$). For two muscles, medial deltoid and teres major, there was an effect of Condition on EMG activity during the CUE period ($.05 > p > .01$). The increased EMG signal observed in these muscles during the plane dissociation condition may have been due to a slight alteration in the animal's starting posture in response to the board placed over its arm. There was, as expected, a main effect of Target for all proximal arm muscles studied during the movement epoch ($p < .01$). MTs between the standard ($M = 173.32$ msec, $SEM = 2.36$ msec) and plane dissociation ($M = 177.37$ msec, $SEM = 3.02$ msec) conditions were not significantly different for monkey B, $t(22) = -1.1$, $p = .282$; however, MTs for monkey G were significantly faster in the plane dissociation condition ($M = 161.16$ msec, $SEM = 1.71$ msec) relative to the standard condition ($M = 198.55$ msec, $SEM = 1.93$ msec), $t(23) = 14.39$, $p < .001$. MTs for monkey B were also not significantly different between the standard ($M = 171.90$ msec, $SEM = 1.93$ msec) and feedback reversal ($M = 175.91$ msec, $SEM = 1.70$ msec) conditions, $t(26) = -1.51$, $p = .144$. Lastly, RTs between the standard ($M = 537.9$ msec, $SEM = 12.82$ msec) and plane dissociation ($M = 522$ msec, $SEM = 9.89$ msec) conditions were not significantly different, $t(45) = .927$, $p = .359$; however, RTs were significantly faster in the standard condition ($M = 571.3$ msec, $SEM = 8.65$ msec) relative to the feedback reversal condition ($M = 717.1$ msec, $SEM = 14.72$ msec), $t(26) = -8.119$, $p < .001$.

Neural Findings

Standard versus Plane Dissociation (Monkeys G and B)

Neural data comparing the standard and plane dissociation conditions were first analyzed separately for each monkey. These data were not different between animals, thus providing justification for pooling our recordings together for the following analyses. A total of 88 task-related single units were recorded during the standard and plane dissociation conditions over 46 recording sessions, 62 from deep sites, and 26 from superficial sites. Our first main observation was that the mean firing rate of cells from deep recording sites tended to decrease in going from the standard condition to the nonstandard plane dissociation condition. An example cell demonstrating this decrease in discharge between conditions, as well as a temporal pattern of modulation reflecting that observed at the population level (i.e., increased activity during early cue and MT) is displayed in Figure 4A. The solid line in Figure 4B displays a cumulative distribution of the mean discharge contrast ratios between the standard and plane dissociation conditions for deep cells.

Examining this distribution reveals that the majority (>70%) of deep cells exhibited higher discharge rates during the standard condition (i.e., positive contrast ratios), which suggests a dampened output from cells within the IPS and POs during plane-dissociated reaching [repeated-measures ANOVA, main effect of Condition, $F(1, 61) = 10.03$, $p = .0024$; Figure 5A, left]. The population averaged peristimulus time histogram (PSTH) displayed in Figure 5B (left) illustrates this suppression in activity throughout the entire trial. We also observed a significant main effect of epoch, $F(5, 305) = 15.84$, $p < .0001$, but no condition by epoch interaction, $F(5, 305) = 0.74$, $p = .59$. Figure 5A (left) shows that population-level activity is significantly higher during early CUE relative to all other trial epochs (Tukey HSD post hoc multiple comparisons, preCUE: $p = .042$, lCUE: $p = .0007$, RT: $p = .0002$, MT: $p = .026$, TH: $p = .00002$). Note also in this figure that population-level modulation was stronger during preCUE ($p = .028$) and MT ($p = .044$) relative to TH. Thus, on average, cells from deep SPL recording sites were most strongly modulated upon presentation of the reach target, as well as during the reaching movement. Importantly, we found no significant difference in the mean discharge rate of cells from deep sites that were recorded during eye calibration before task execution (i.e., when eye movements alone were made to targets presented on the horizontal versus vertical monitors, $t(33) = -.204$, $p = .839$).

Cells from superficial recording sites also displayed a significant main effect of Epoch [repeated-measures ANOVA, $F(5, 125) = 5.49$, $p = .0001$], with no Condition × Epoch interaction, $F(5, 125) = 2.09$, $p = .07$. A salient difference, however, was that, unlike deep cells, superficial cells did not tend to decrease their discharge rate when the plane of the hand movement and the plane of gaze were dissociated [main effect of Condition, $F(1, 25) = 0.28$, $p = .602$]. The dashed line in Figure 4B displays the cumulative distribution of mean discharge contrast ratios between standard and plane dissociation conditions for superficial cells, demonstrating an equal proportion of negative and positive contrast ratios. Averaged data from each epoch for superficial recordings is displayed in Figure 5A (right), demonstrating no significant difference between conditions, while the only significant difference between epochs was a greater discharge rate during early CUE relative to TH (Tukey HSD post hoc analyses, $p = .011$). The population averaged PSTH for superficial cells

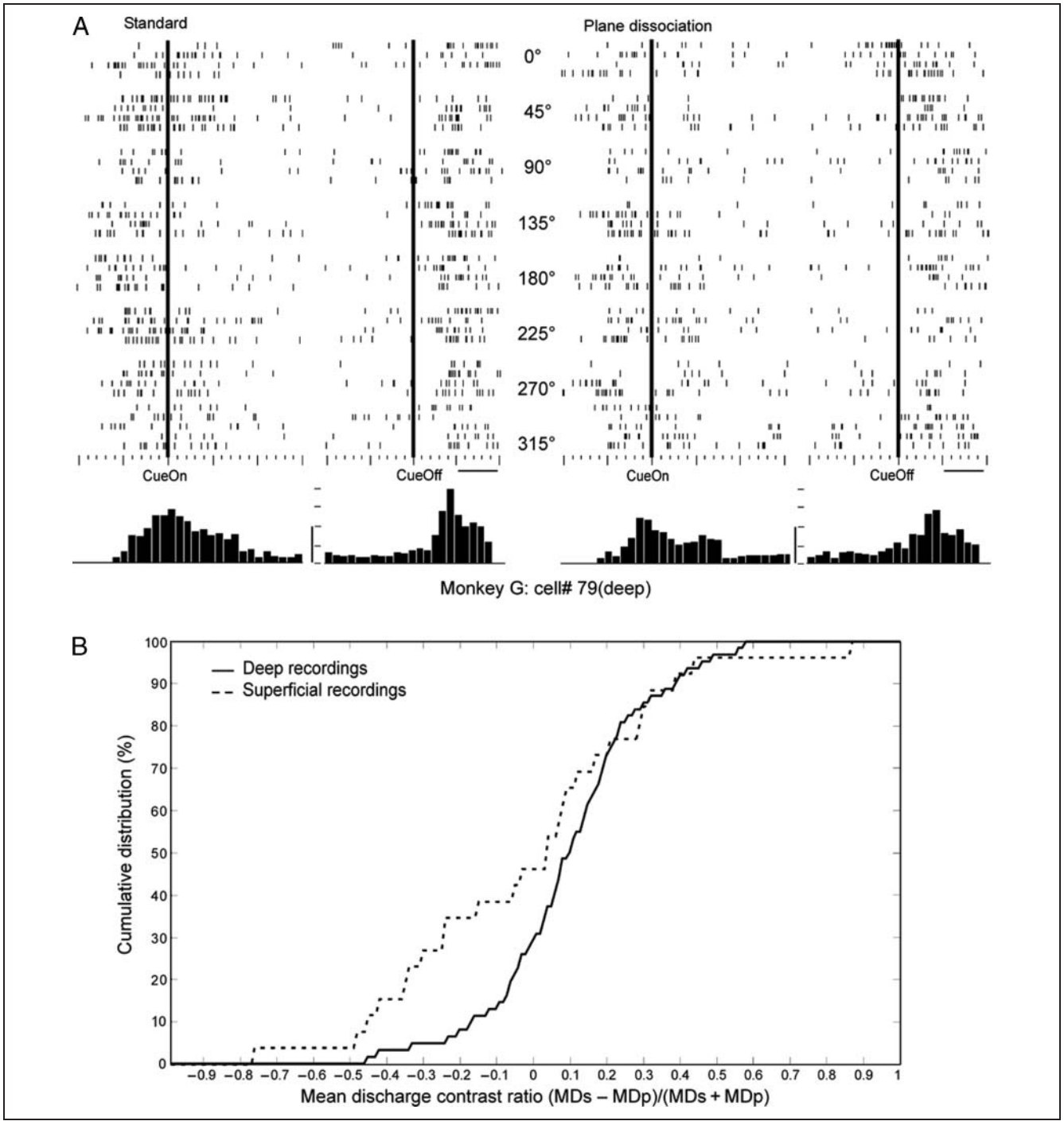

Figure 4. Example cell from deep recording site and cumulative distributions of mean discharge contrast ratios. (A) Raster plots and peristimulation time histograms (PSTHs; 100-msec bins) displaying neural activity of a deep cell recorded from monkey G during the standard and plane dissociation conditions. Plots are double-aligned to presentation (CueOn) and disappearance (CueOff/go signal) of the reach target. Horizontal scale bar: 500 msec. Vertical scale bar: 17 spikes/sec. In the standard condition raster plot, note the emergence of directional preference (PD: 0–45°; non-PD: 90–180°) upon presentation of the reach target, which is absent during the plane dissociation condition (along with an overall reduction in firing rate). (B) MDs represents mean discharge during the standard condition; MDp represents mean discharge during the plane dissociation condition.

illustrates a tendency toward increased activity during the plane dissociation condition (Figure 5B, right); however, this increase did not reach significance in our statistical analysis. Thus, superficial cells exhibited some increased activation upon presentation of the reach target, but no significant difference in mean discharge between conditions. When comparing normalized mean discharge rates in deep versus superficial recording sites (i.e., Figure 5, left versus right), deep cells exhibited significantly higher activation (M = 21.20, SEM = 1.08) than superficial cells (M = 13.32, SEM = 1.67) during the standard condition (MD = 7.89, $p < .001$), while no significant difference in

mean discharge rate between recording sites was observed during the plane dissociation condition [deep: $M = 18.21$, $SEM = 1.12$; superficial: $M = 14.53$, $SEM = 1.72$; condition by recording site interaction: $F(1, 86) = 4.09$, $p = .046$]. These results reflect a reversal in condition-related modulation between the two recording sites, with deep cells responding preferentially to the standard condition and superficial cells exhibition lower overall activation, but responding preferentially to the plane dissociation condition.

Significant directional tuning in at least one epoch was observed in 50% (31/62) of deep recordings and 35% (9/26) of superficial recordings. Significant directional preference tended to be transient, typically reaching significance only during one trial epoch (often during CUE, however, also during RT and MT). Notably, a large proportion of both deep (45%) and superficial (56%) cells exhibited significant directional tuning during the standard condition but not during the plane dissociation condition. Comparing vector lengths between conditions in these cells revealed a significant decrease in tuning strength during the plane dissociation condition relative to the standard condition [$t(27) = -9.09$, $p < .001$]. Figure 6A displays the tuning curves of example cells exhibiting this decrease in tuning strength between conditions. In some cases, the change in tuning strength appears to be due to a reduced firing rate during the plane dissociation condition (e.g., cells 78b, 95a, 111a, 20, and 28b), whereas in other cases directional preference actually appears to be lost (e.g., cells 90b, 111b, 11b, and 29b). There were also many cells that showed the opposite behavior by exhibited significant directional tuning during the plane dissociation condition but not during the standard condition. Comparing vector lengths between conditions in these cells revealed a significant increase in tuning strength during the plane dissociation condition relative to the standard condition [$t(13) = 8.94$, $p < .001$]. A small proportion of cells also maintained significant directional tuning in both conditions. A comparison of directional tuning vector lengths between the standard and plane dissociation conditions for all cells exhibiting significant tuning in at least one condition can be seen in Figure 6B.

Standard versus Feedback Reversal (Monkey B Only)

A total of 62 task-related single units were recorded during the standard and feedback reversal conditions over 27 recording sessions, 26 from deep sites, and 36 from superficial sites. For this comparison, we observed no main effect of Condition on the firing rate of cells from deep recording sites [repeated-measures ANOVA, $F(1, 25) = 0.75$, $p = .396$]. That is, unlike in the nonstandard condition

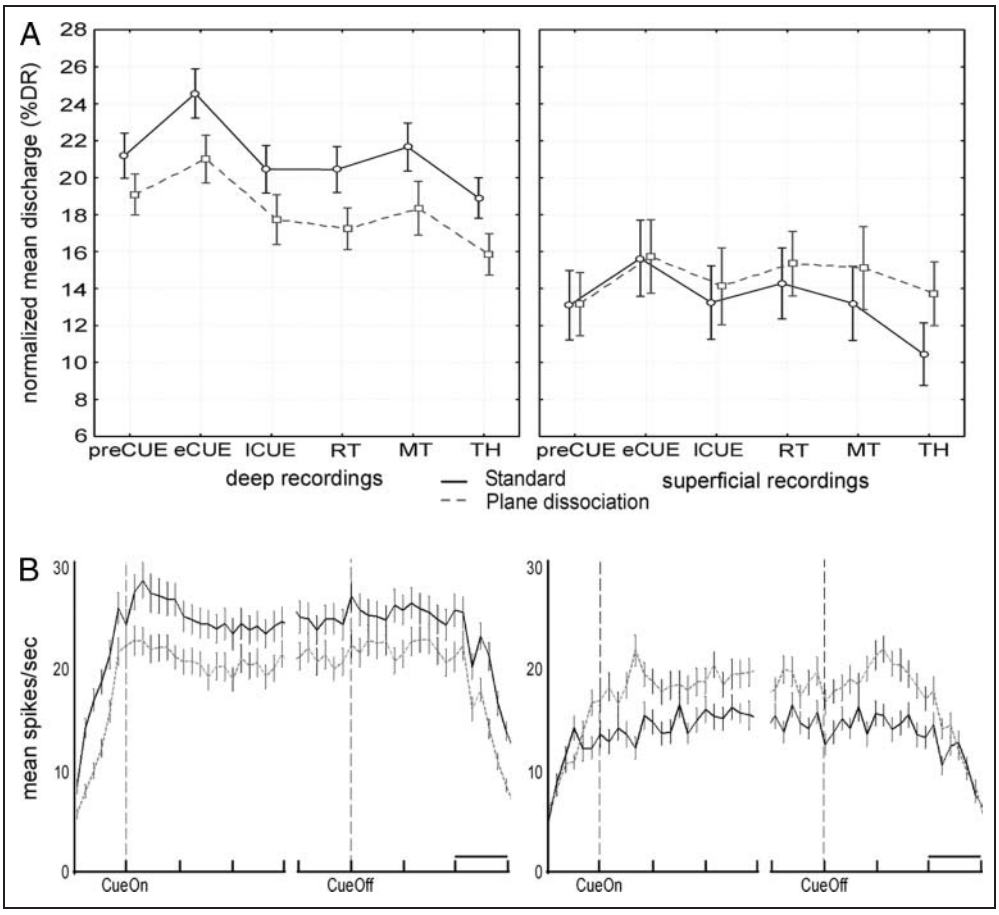

Figure 5. Population-averaged comparisons between the standard and plane dissociation conditions. (A) Normalized mean discharge rates (%DR) as a function of trial epoch and parietal area. (B) Population averaged PSTHs (100-msec bins) double-aligned to presentation (CueOn) and disappearance (CueOff/go signal) of the reach target. Horizontal scale bar: 500 msec. Vertical bars denote ±1 *SEM*.

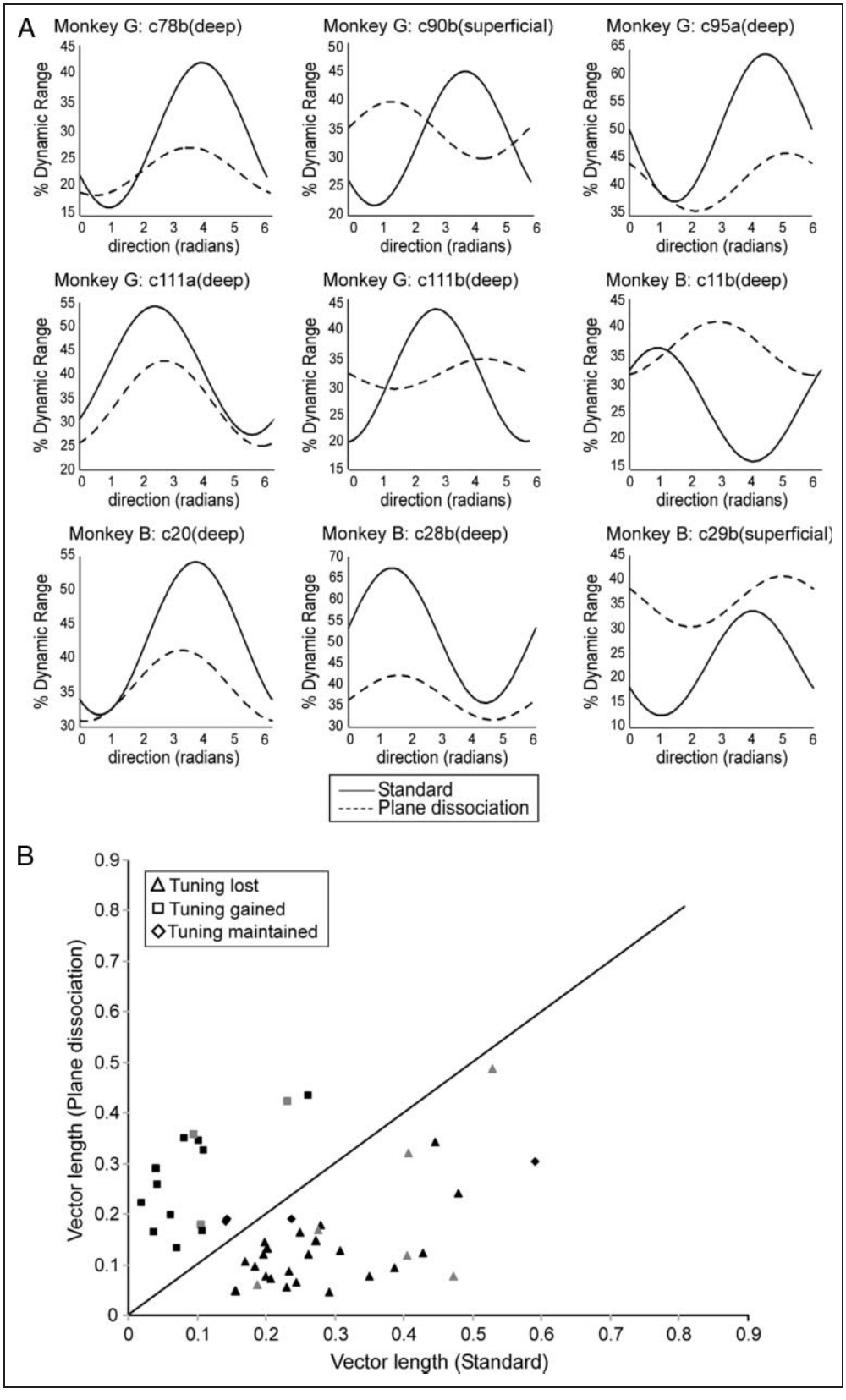

Figure 6. Directional tuning curves and depth of tuning scatter plot. (A) Example cells from both animals and both recording sites exhibiting decreased tuning strength between the standard and plane dissociation conditions. (B) Vector lengths of all cells exhibiting significant directional tuning in at least one condition. Black: deep recording sites. Gray: superficial recording sites.

involving movements made in a different spatial plane from the visual target, cells from deep recording sites did not reduce their discharge rate relative to the standard condition when the cursor visual feedback was rotated by 180°.

Figure 7A displays an example cell from a deep recording site demonstrating a similar discharge rate between the standard and feedback reversal conditions, but suppression in discharge during the plane dissociation condition. By

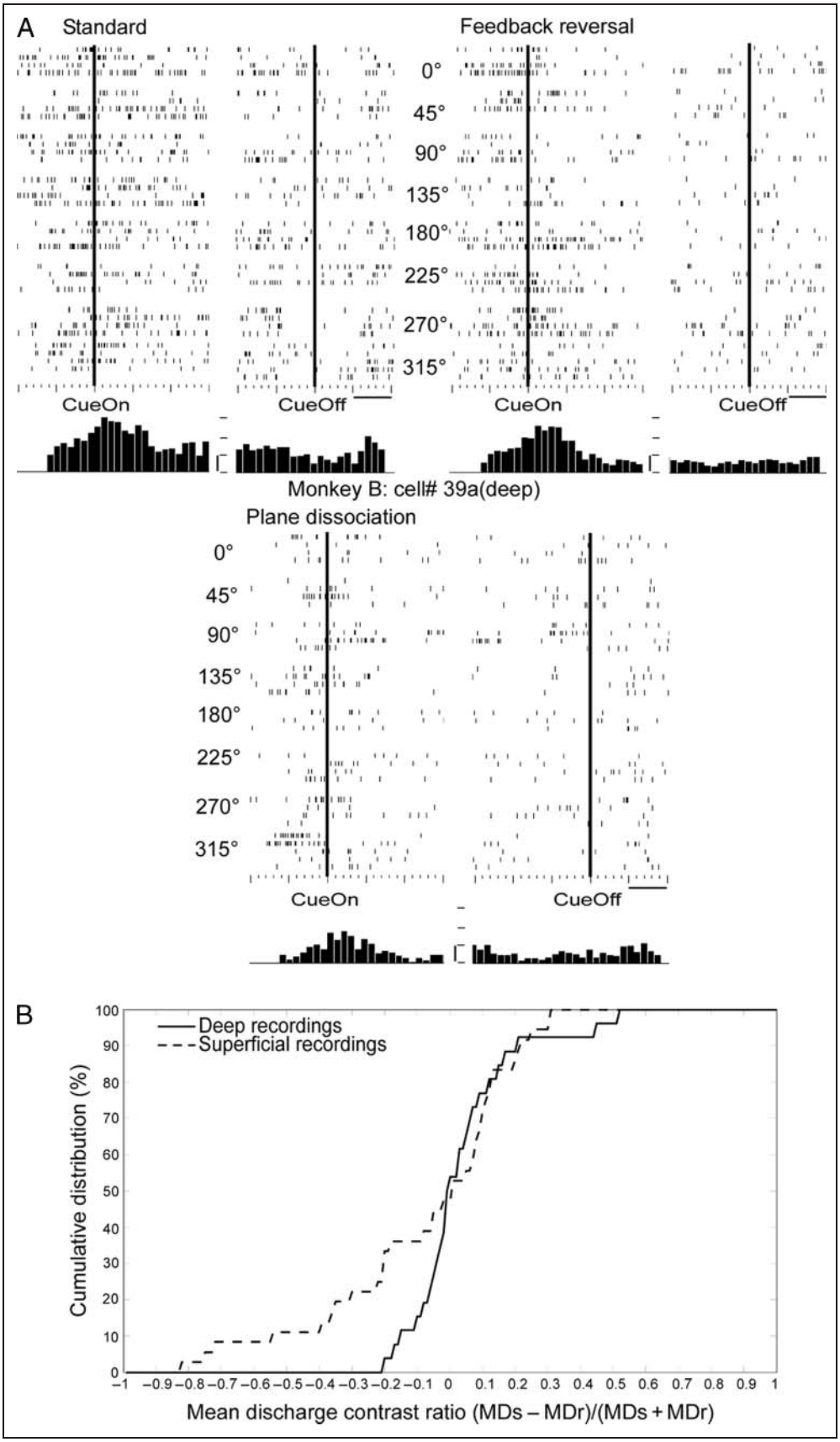

Figure 7. Example cell from deep recording site and cumulative distributions of mean discharge contrast ratios. (A) Raster plots and raw spike histograms (100-msec bins) displaying neural activity of a deep cell recorded from monkey B during the standard, plane dissociation, and feedback reversal conditions. Plots are double-aligned to the presentation (CueOn) and disappearance (CueOff/ go signal) of the reach target. Horizontal scale bar: 500 msec. Vertical scale bar: 10 spikes/sec. In the feedback reversal raster plot, note the shift and strengthening of directional preference upon cue presentation (PD: 180–270°) relative to the standard raster plot (non-PD: 180–225°). Also note the overall decrease in firing rate during the plane dissociation condition. (B) MDs represents mean discharge during the standard condition; MDr represents mean discharge during the feedback reversal condition.

examining the solid cumulative distribution line in Figure 7B, we can see that the majority of cells from deep recording sites did not exhibit large alterations in firing rate between the standard and feedback reversal conditions. We did however observe a main effect of epoch on normalized mean discharge rate in deep recordings, like that observed for the plane dissociation versus standard comparison, $F(5, 125) = 13.92$, $p < .0001$, as well as no condition by epoch interaction, $F(5, 125) = 1.76$, $p = .125$. Figure 8A (left) demonstrates the overall similarity in firing rate between the standard and feedback reversal conditions for deep cells as well as significantly higher population-level activity during early CUE relative to late CUE ($p = .0001$), RT ($p = .0003$), and TH ($p = .001$), but not MT (Tukey HSD post hoc multiple comparisons). An increased population-level discharge rate can also be seen during preCUE relative to late CUE ($p = .011$) and RT ($p = .024$). The similarity in firing rate between conditions and temporal modulation throughout the trial can also be seen in the population averaged PSTH plotted for deep recording sites (Figure 8B, left). These results indicate that cells from within the IPS and POs were most strongly modulated in anticipation and upon presentation of the reach target, as well as during the reaching movement (similar to the plane dissociation versus standard task comparison). However, the mean discharge rate of cells from deep recording sites was not affected by a 180° rotation in the required hand movement relative to the visual target.

The behavior of cells from superficial recordings during the feedback reversal comparison was similar to that observed for the plane dissociation comparison. That is, we found no main effect of condition, $F(1, 35) = 3.21$, $p = .082$, and no condition by epoch interaction, $F(5, 175) = 1.45$, $p = .207$. However, we did observe a significant main effect of Epoch on normalized mean discharge rate [repeated-measures ANOVA, $F(5, 175) = 18.99$, $p < .0001$]. Specifically, cells recorded from superficial sites displayed higher population-level activity during early CUE relative to preCUE ($p = .0004$), MT ($p = .019$), and TH ($p = .00002$). Furthermore, the population-averaged discharge rate was significantly higher during late CUE ($p = .002$), RT ($p = .0002$), and MT ($p = .0083$) relative to TH (Tukey HSD post hoc analyses). Figure 8A (right) illustrates this modulation upon presentation of the reach target, but not to the same extent as cells from deep recordings (left). It is also apparent from the dashed cumulative distribution line in Figure 7B and the population-averaged PSTH (Figure 8B, right) that cells from superficial sites tended to be more responsive during the feedback reversal condition, although this observation was not significant (ANOVA, $p = .082$). When comparing mean discharge rates in deep versus superficial recording sites (i.e., Figure 8, left versus right), deep cells exhibited significantly higher activation ($M = 21.67$, $SEM = 1.71$) than superficial cells ($M = 14.34$, $SEM = 1.45$) during the standard condition ($MD = 7.33$, $p = .002$), whereas no significant difference in mean discharge rate between recording sites was observed during the feedback reversal condition [deep: $M = 20.57$, $SEM = 1.70$; superficial: $M = 16.92$, $SEM = 1.44$; trend toward condition by recording site interaction: $F(1,$

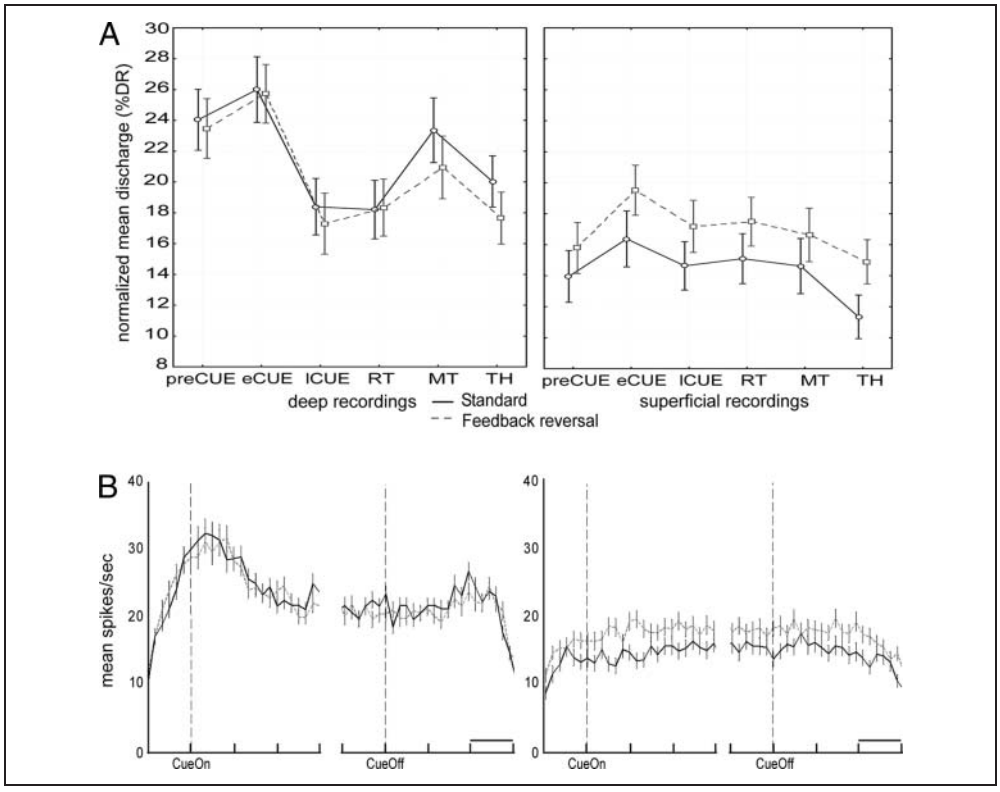

Figure 8. Population-averaged comparisons between the standard and feedback reversal conditions. (A) Normalized mean discharge rates (%DR) as a function of trial epoch and parietal area. (B) Population-averaged PSTHs (100-msec bins) double-aligned to presentation (CueOn) and disappearance (CueOff/go signal) of the reach target. Horizontal scale bar: 500 msec. Vertical bars denote ±1 *SEM*.

60) = 3.34, $p = .07$]. These results reflect higher overall activation in deep cells relative to superficial cell, with preferential activation in superficial cells during the feedback reversal condition.

Significant directional tuning in at least one epoch was observed in 46% (12/26) of deep recordings and 33% (12/36) of superficial recordings. As observed in the standard versus plane dissociation comparison, a large proportion of both deep (50%) and superficial (42%) cells exhibited reduced tuning strength in going from the standard to the feedback reversal condition [$t(17) = -6.64$, $p < .001$]. The tuning curves of three example cells exhibiting this decrease in tuning strength are displayed in Figure 9A (top). There were also many cells that demonstrated an increase in tuning strength in going from the standard to the feedback reversal condition [$t(12) = 7.96$, $p < .001$], as well as a small proportion of both deep and superficial cells that maintained significant directional tuning and a similar tuning strength in both conditions.

Importantly, all cells exhibiting significant tuning in both conditions showed a shift in their PD close to 180° (168.3° ± 17.5°), indicating that the directional tuning of these cells remained constant with respect to the spatial reach goal (which also rotated 180° between conditions), but shifted with respect to the direction of the visual target (which did not change between conditions). Tuning curves and polar plots for two example cells are displayed in Figure 9A (bottom). A comparison of directional tuning vector lengths between the standard and feedback reversal conditions for all cells exhibiting significant tuning in at least one condition can be seen in Figure 9B.

DISCUSSION

Our results demonstrate that changes in SPL cell discharge rates and directional tuning do indeed occur as a function of visuomotor compatibility, which suggests the involvement of this brain region in nonstandard rule-based visuomotor control. Specifically, we observed significant suppression in activity during plane dissociated reaching and maintenance of directional tuning with respect to the reach goal during a feedback reversal task. We also observed increased neural activity in deep SPL cells during early reach planning and movement execution across all tasks. Here we consider the implications of these findings.

Parietal Contribution to Reach Control When Eye and Hand Movements Are Spatially Incongruent

The temporal pattern of activity observed in deep recordings (i.e., increased discharge during early CUE and MT) appears to reflect the neuronal properties that others have described for areas MIP (within the IPS) and V6A (within the POs; Fattori, Kutz, Breveglieri, Marzocchi, & Galletti, 2005; Fattori, Gamberini, Kutz, & Galletti, 2001). The modulation observed across tasks in the current study suggests that cells in these areas may play a role in early reach planning and on-line reach monitoring during both standard and nonstandard reaching tasks. Increased discharge during early CUE (when gaze is on the central target) also suggests that these cells are modulated in response to presentation of a visual target in the peripheral field, which is consistent with the V6A visual topography described by Galletti and colleagues (1999).

It is known that SPL cells receive convergent visual and proprioceptive input, and it has been suggested that these cells relate target information in retinocentric coordinates to the current posture of the limb in body-centered coordinates (Kalaska & Crammond, 1995; Ferraina & Bianchi, 1994; Caminiti, Johnson, Galli, Ferraina, & Burnod, 1991; Caminiti, Johnson, & Urbano, 1990). During a plane dissociated reach, however, the target location in retinocentric coordinates provides invalid information about the reach goal, which would need to be inhibited to reach toward the correct spatial location. In a fMRI study, Gorbet and colleagues (2004) also observed a decrease in activity within the superior parietal-frontal reach network during nonstandard visuomotor transformations and suggested that this decrease may reflect inhibition of a default network for standard reaches. In other words, because the visual target does not indicate the spatial goal of the required reach in the plane dissociation condition, inhibition of the neural processes involved in natural eye–hand congruent reaches may be required. Such suppression in parietal activity may be driven by incongruent visual and proprioceptive inputs during the plane-dissociated task, which suggests that plane-dissociated reaching may rely on implicit (bottom–up) sensorimotor recalibration.

The observation that cells recorded from superficial sites responded differently from those recorded in the sulcus is not surprising considering previous research demonstrating that the SPL is not functionally homogeneous. For example, previous studies have shown that superficial cells in more anterior parts of the SPL (e.g., area PEc) tend to respond during passive movements and later on during the course of active movements (Johnson et al., 1996; Burbaud, Doegle, Gross, & Bioulac, 1991; Chapman, Spidalieri, & Lamarre, 1984). Furthermore, anterior parietal areas outside the IPS have been shown to become active only after the effector for movement is selected, unlike areas within the IPS that are active when effector information is ambiguous (Cui & Andersen, 2011; Beurze, de Lange, Toni, & Medendorp, 2007, 2009; Medendorp, Goltz, Crawford, & Vilis, 2005). Area PEc is also closely connected with the primary somatosensory and motor cortices, as well as the caudal dorsal premotor (PMd) cortex (Johnson et al., 1996), placing it in an ideal position for the further processing of reafferent information arising during movement and the guidance of movement using somesthetic feedback (Breveglieri, Galletti, Monaco, & Fattori, 2007; Breveglieri, Galletti, Gamberini, Passarelli, & Fattori, 2006; Kalaska, 1996; Weinrich, Wise, & Mauritz, 1984). In the current study, the tendency toward increased firing rates

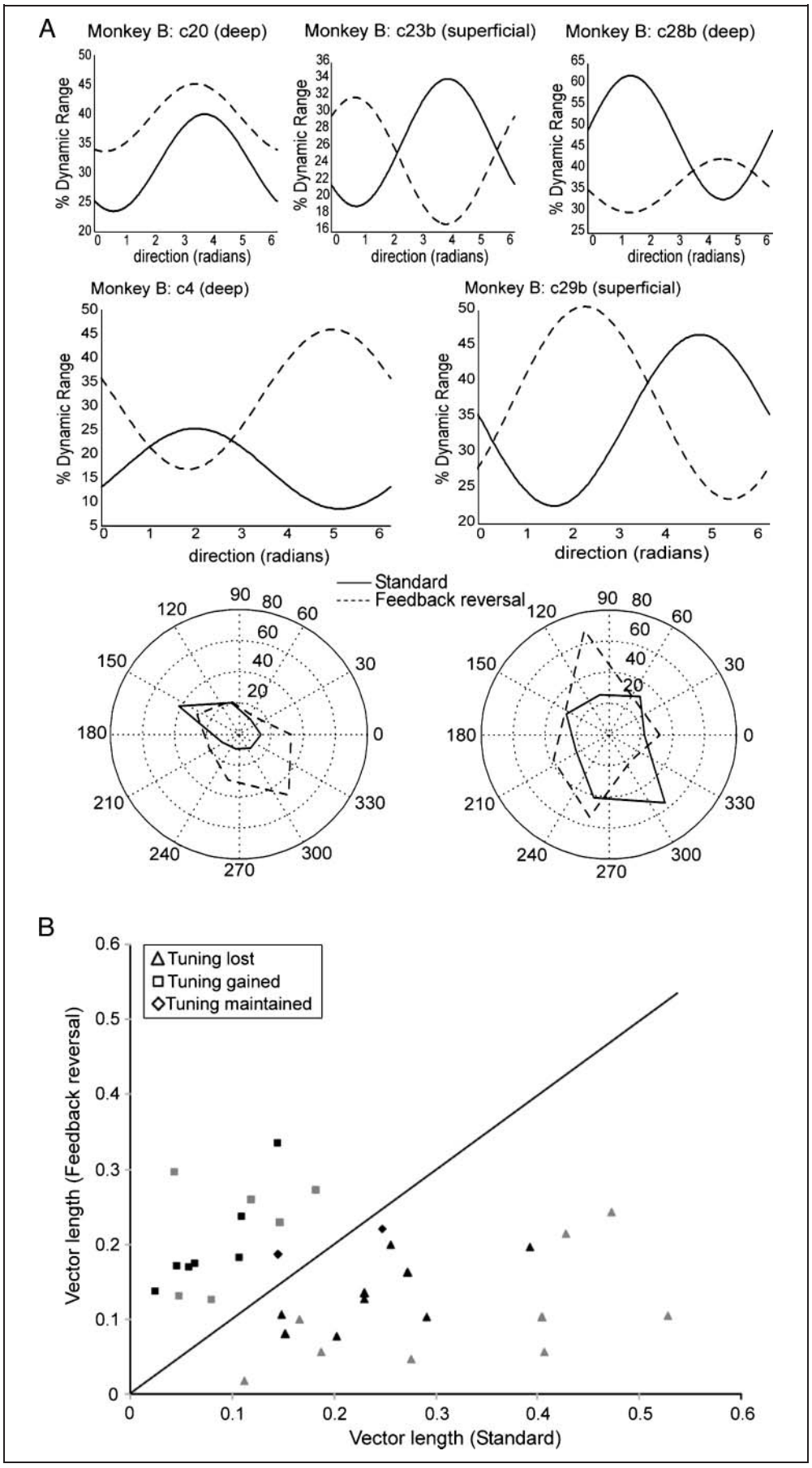

Figure 9. Directional tuning curves, polar plots, and depth of tuning scatter plot. (A) Top: Three example cells exhibiting decreased tuning strength between the standard and feedback reversal conditions. Bottom: Tuning curves and polar plots for two example cells exhibiting maintenance in directional tuning with respect to spatial reach goal, but 180° shift with respect to the visual target. (B) Vector lengths of all cells exhibiting significant directional tuning in at least one condition. Black: deep recording sites. Gray: superficial recording sites.

in superficial cells during the nonstandard conditions, especially during movement and TH (see Figures 5 and 8, right), may reflect increased reliance on somesthetic feedback to calibrate eye–hand coordination while moving and positioning the hand, which could not be constantly monitored by vision during these tasks (Vercher et al., 1994; Gauthier & Mussa-Ivaldi, 1988).

In contrast, deep cells in the more posterior (V6A) and medial (MIP) regions of the SPL have been shown to respond during the delay period before movement onset and to project to more anterior motor areas (i.e., rostral PMd) involved in response selection and planning (Johnson et al., 1996; Kalaska, 1996; Colby, Gattass, Olson, & Gross, 1988; Weinrich et al., 1984). Thus, these regions of the SPL are likely involved in generating the internal estimates necessary for the feedforward guidance of rule-based motor behavior.

The finding that many of the SPL cells recorded in the current study display activity that varies with movement direction (i.e., exhibit significant directional tuning) is consistent with previous research (Fattori et al., 2005; Burbaud et al., 1991; Mackay & Crammond, 1987; Burbaud, Gross, & Bioulac, 1985; Chapman et al., 1984; Seal, Gross, Doudet, & Bioulac, 1983; Seal, Gross, & Bioulac, 1982; Bioulac & Lamarre, 1979). Furthermore, the directional tuning results in the current study suggest a functional dissociation between superficial and deep recordings, with more directionally tuned responses observed in deep cells relative to superficial cells. These results are in accordance with Johnson and colleagues (1996) and suggest that cells within the IPS and POs are more sensitive to reach direction than cells on the gyrus.

The observation in the current study that many cells reduce their tuning strength between the standard and nonstandard tasks, whereas some cells increase their tuning strength is consistent with findings reported by Marzocchi, Breveglieri, Galletti, and Fattori (2008). These authors demonstrated that many cells in area V6A respond during reaches directed toward the spatial location of the animal's gaze (i.e., standard reaches), whereas other cells respond preferentially during reaches directed away from the location of the animal's gaze (as is the case for plane dissociated and feedback reversal reaches). Furthermore, Fattori and colleagues (2001) have observed that when V6A cells are not active during reaches performed under visual control they often become active when reaching outside the field of view. In other words, the larger proportion of cells that exhibited significant directional tuning during the standard task in the current study may use visual information to code for the direction of eye–hand congruent reaches, whereas those cells exhibiting significant directional tuning during the nonstandard tasks may integrate proprioceptive information to encode directionality when the visual target and reach goal are incongruent. These results suggest that different groups of cells encode the reach vector for eye–hand congruent versus eye–hand incongruent reaches. Considering the greater propensity for eye–hand congruent behaviors performed in natural settings, it is not surprising that we observed more cells with increased tuning strength during standard reaching in the current study.

Parietal Contributions to Nonstandard Reaches Involving 180° Visual Feedback Reversal

The similarity in mean discharge rate observed between standard and feedback reversal conditions in the current study suggests that deep parietal cells may be using a context-dependent spatial reach goal to prepare the intended movement, which would render the standard and feedback reversal conditions indistinguishable from one another. To do this, SPL cells would have to incorporate contextual knowledge about the requirement to move in the opposite direction of the visual target into the reach plan during the feedback reversal condition. The neural processing involved in selecting and implementing this goal to move in the opposite direction may occur in frontal areas (e.g., supplementary and cingulate motor areas), which have been shown to be modulated during movement goal selection in a symbolically cued task (Diedrichsen, Grafton, Albert, Hazeltine, & Ivry, 2006). In other words, performing the feedback reversal task may rely on explicit (top–down) strategic control. The observation in the current study that all cells exhibiting significant directional tuning in both conditions changed their PDs by approximately 180° between conditions provides evidence for the integration of an opposite reach rule at the single cell level. These results suggest that spatially tuned SPL cells encode the intended reach direction (as opposed to the visual target) in the feedback reversal task. Furthermore, the RT delay observed in the feedback reversal condition may reflect the increased information processing time required to integrate cognitive information regarding the opposite reach rule from frontal areas with perceptual-motor information in parietal areas when the reach goal is not directly specified by the visual target (Diedrichsen et al., 2006; Brass, Ullsperger, Knoesche, von Cramon, & Phillips, 2005; Stoet & Snyder, 2004).

The observation that cells in the SPL change their directional tuning by approximately 180° in the feedback reversal task is consistent with recent findings by Gail and colleagues (2009). These authors demonstrated that cells in both PRR and PMd respond to the motor goal for both pro- and anti-reaches. Similar results have also been reported by Kalaska (1996), who observed that during a "redirected delay" (i.e., anti-reach) task, SPL and PMd cells show a brief response to the visual cue presented in their PD (as determined during a "direct delay" condition), but within 250 msec, these cells show a complete reversal in sign (i.e., activity is suppressed in the direction of the visual cue). By the end of the delay period, the activity of these cells reflected the intention of the monkey to move toward a spatial goal in the opposite direction of the instructional cue. Kalaska (1996) suggests that this

delay period activity reflects central processes that recognize the movement goal signaled by the cue rather than a passive response to the location of the visual cue itself. Thus, the directional tuning modulation observed during redirected delay trials appears to contribute to the remapping between target location and movement in the opposite direction. This is in contrast to a human fMRI study in which most SPL areas retained visual tuning after reversing prism adaptation (Fernandez-Ruiz, Goltz, DeSouza, Vilis, & Crawford, 2007); however, this might be accounted for by different neural processes involved in consciously reversing the reach goal versus unconscious sensorimotor adaptation (Crawford et al., 2011).

Study Limitations

Because eye and hand movements occur at the same time in the current study, the possibility that our results reflect eye movement related activity must be considered. For example, decreased neural activity between the standard and plane dissociation conditions in the current study might be explained by the shift in gaze between conditions (Crawford et al., 2011; Blohm & Crawford, 2009). To account for this, we tested the potential contribution of eye movements alone to the difference in neural discharge observed between the standard and plane dissociation conditions and found no significance (see Results). Thus, the decrease in mean discharge observed in deep cells during the plane dissociation condition cannot be explained solely by the change in eye position between the two tasks. In other words, the observed decrease in discharge during the plane dissociated task occurred only when both the eyes and the hand were involved.

Cells with visual properties are known to exist throughout the SPL; thus, to avoid the inclusion of purely visual cells in the current study, action potentials were isolated and considered task-related only when their activation was modulated during reaches toward a visual stimulus and not during visual observation alone. It should also be noted that had we required fixation throughout the experiment it may have confounded our results by necessitating increased peripheral attention and active suppression of natural eye movements toward the visual targets (Culham & Kanwisher, 2001). The conditions in the current study were designed to allow natural eye–hand coordination with respect to time while evaluating neuronal modulation resulting from manipulation of the spatial congruence between the eyes and the hand.

The reach requirements of all three conditions were identical, and the animals were highly trained on our experimental tasks; however, reach trajectory variations were still observed, with slight differences between conditions (Figure 3). Eliminating these reach trajectory differences may not have been possible considering psychophysical evidence in humans demonstrating that the kinematics of nonstandard eye–hand incongruent reaches tend to differ from those of standard reaches, even when they are well learned (Gorbet & Sergio, 2009; Henriques et al., 1998; Prablanc et al., 1979). With this said, the high similarity in EMG activity observed across conditions in the current study suggests that the biomechanics (i.e., intrinsic parameters) of the reaching behaviors were kept constant in all three tasks. Thus, the differences in neural activity observed can be attributed to the manipulation of extrinsic task parameters (i.e., dissociation of the visual target from the reach goal).

Lastly, our results for the feedback reversal condition were based on cell recordings from only one animal, which we were unable to test in our second animal. Although these findings require replication, their consistency with previous studies merits reporting. Furthermore, data recorded in the other two conditions were similar between our two animals, suggesting that the same would be true for the third condition. Importantly however, we are unable to confirm that the feedback reversal results do not reflect an unusual behavioral strategy employed by the single animal examined in this condition.

Conclusions

Our results suggest that cells from within the IPS and POs are involved in preparing an upcoming reach, as well as monitoring and updating that reach during execution. Our results also support the notion that habitual networks for eye–hand congruent reaching may need to be inhibited when visual and reach targets are in different spatial planes. Furthermore, in the context of the 180° feedback reversal task, our results suggest that SPL cells can incorporate cognitive information into the movement plan allowing them to encode the spatial goal of the upcoming reach as opposed to the visual target. Taken together, these findings suggest that SPL cells play an important role in processing information about the learned nonstandard nature of a task. Such context-dependent information allows for appropriate motor output through the integration of different rules in different situations.

Acknowledgments

We would like to thank Taiwo McGregor, Tyrone Lew, and Dr. Hongying Wang for their exceptional technical and surgical assistance, as well as Natasha Down, Veronica Scavo, and Julie Panakos for their invaluable animal care expertise. This work was supported by the Canadian Institutes of Health Research (grant MOP-74634 to L. S.); the Canadian Foundation for Innovation and the Ontario Innovation Trust (to L. S.); the Natural Sciences and Engineering Research Council (NSERC Canadian graduate scholarship to K. H.); and the Canadian Federation of University Women (CFUW memorial fellowship to K. H.). J. D. Crawford was supported by a Canada Research Chair.

Reprint requests should be sent to Lauren E. Sergio, School of Kinesiology and Health Science, York University, 4700 Keele Street, Toronto, Ontario, M3J 1P3, Canada, or via e-mail: lsergio@yorku.ca.

REFERENCES

Archambault, P. S., Caminiti, R., & Battaglia-Mayer, A. (2009). Cortical mechanisms for on-line control of hand movement trajectory: The role of the posterior parietal cortex. *Cerebral Cortex, 19,* 2848–2864.

Archambault, P. S., Ferrari-Toniolo, S., & Battaglia-Mayer, A. (2011). Online control of hand trajectory and evolution of motor intention in the parietofrontal system. *Journal of Neuroscience, 31,* 742–752.

Battaglia-Mayer, A., Ferraina, S., Mitsuda, T., Marconi, B., Genovesio, A., Onorati, P., et al. (2000). Early coding of reaching in the parietooccipital cortex. *Journal of Neurophysiology, 83,* 2374–2391.

Beurze, S. M., de Lange, F. P., Toni, I., & Medendorp, W. P. (2007). Integration of target and effector information in the human brain during reach planning. *Journal of Neurophysiology, 91,* 188–199.

Beurze, S. M., de Lange, F. P., Toni, I., & Medendorp, W. P. (2009). Spatial and effector processing in the human parietofrontal network for reaches and saccades. *Journal of Neurophysiology, 101,* 3053–3062.

Bioulac, B., & Lamarre, Y. (1979). Activity of postcentral cortical neurons of the monkey during conditioned movements of a deafferented limb. *Brain Research, 172,* 427–437.

Blohm, G., & Crawford, J. D. (2009). Fields of gain in the brain. *Neuron, 64,* 598–600.

Bo, J., Contreras-Vidal, J. L., Kagererm, F. A., & Clark, J. E. (2006). Effects of increased complexity of visuo-motor transformations on children's arm movements. *Human Movement Science, 25,* 553–567.

Braak, H., & Braak, E. (1991). Neuropathological staging of Alzheimer-related changes. *Acta Neuropathologica, 82,* 239–259.

Brass, M., Ullsperger, M., Knoesche, T. R., von Cramon, D. Y., & Phillips, N. A. (2005). Who comes first? The role of the prefrontal and parietal cortex in cognitive control. *Journal of Cognitive Neuroscience, 17,* 1367–1375.

Breveglieri, R., Galletti, C., Gamberini, M., Passarelli, L., & Fattori, P. (2006). Somatosensory cells in area PEc of macaque posterior parietal cortex. *Journal of Neuroscience, 26,* 3679–3684.

Breveglieri, R., Galletti, C., Monaco, S., & Fattori, P. (2007). Visual, somatosensory, and bimodal activities in the macaque parietal area PEc. *Cerebral Cortex, 18,* 806–816.

Bunge, S. A., Wallis, J. D., Parker, A., Brass, M., Crone, E. A., Hoshi, E., et al. (2005). Neural circuitry underlying rule use in humans and nonhuman primates. *Journal of Neuroscience, 25,* 10347–10350.

Burbaud, P., Doegle, C., Gross, C., & Bioulac, B. (1991). A quantitative study of neuronal discharge in areas 5, 2, and 4 of the monkey during fast arm movements. *Journal of Neurophysiology, 66,* 429–443.

Burbaud, P., Gross, C., & Bioulac, B. (1985). Peripheral inputs and early unit activity in area 5 of the monkey during a trained forelimb movement. *Brain Research, 337,* 341–346.

Caminiti, R., Johnson, P. B., Galli, C., Ferraina, S., & Burnod, Y. (1991). Making arm movements within different parts of space: The premotor and motor cortical representation of a coordinate system for reaching to visual targets. *Journal of Neuroscience, 11,* 1182–1197.

Caminiti, R., Johnson, P. B., & Urbano, A. (1990). Making arm movements within different parts of space: Dynamic aspects in the primate motor cortex. *Journal of Neuroscience, 10,* 2039–2058.

Chapman, C. E., Spidalieri, G., & Lamarre, Y. (1984). Discharge properties of area 5 neurones during arm movements triggered by sensory stimuli in the monkey. *Brain Research, 309,* 63–77.

Colby, C. L., Gattass, R., Olson, C. R., & Gross, C. G. (1988). Topographical organization of cortical afferents to extrastriate visual area PO in the macaque: A dual tracer study. *Journal of Comparative Neurology, 269,* 392–413.

Colby, C. L., & Goldberg, M. E. (1999). Space and attention in parietal cortex. *Annual Review of Neuroscience, 22,* 319–349.

Crawford, J. D., Henriques, D. Y. P., & Medendorp, W. P. (2011). Three-dimensional transformations for goal-directed action. *Annual Review of Neuroscience, 34,* 309–331.

Crutcher, M. D., & Alexander, G. E. (1990). Movement-related neuronal activity selectively coding either direction or muscle pattern in three motor areas of the monkey. *Journal of Neurophysiology, 64,* 151–163.

Cui, H., & Andersen, R. A. (2011). Different representations of potential and selected motor plans by distinct parietal areas. *Journal of Neuroscience, 31,* 18130–18136.

Culham, J. C., & Kanwisher, N. G. (2001). Neuroimaging of cognitive functions in human parietal cortex. *Current Opinion in Neurobiology, 11,* 157–163.

Desmurget, M., Epstein, C. M., Turner, R. S., Prablanc, C., Alexander, G. E., & Grafton, S. T. (1999). Role of the posterior parietal cortex in updating reaching movements to a visual target. *Nature Neuroscience, 2,* 563–567.

Diedrichsen, J., Grafton, S., Albert, N., Hazeltine, E., & Ivry, R. B. (2006). Goal-selection and movement-related conflict during bimanual reaching movements. *Cerebral Cortex, 16,* 1729–1738.

Fattori, P., Gamberini, M., Kutz, D. F., & Galletti, C. (2001). "Arm-reaching" neurons in the parietal area V6A of the macaque monkey. *European Journal of Neuroscience, 13,* 2309–2313.

Fattori, P., Kutz, D. F., Breveglieri, R., Marzocchi, N., & Galletti, C. (2005). Spatial tuning of reaching activity in the medial parietal-occipital cortex (area V6A) of macaque monkey. *European Journal of Neuroscience, 22,* 956–972.

Fernandez-Ruiz, J., Goltz, H. C., DeSouza, J. F. X., Vilis, T., & Crawford, J. D. (2007). Human parietal "reach region" primarily encodes intrinsic visual direction, not extrinsic movement direction, in a visual motor dissociation task. *Cerebral Cortex, 17,* 2283–2292.

Ferraina, S., & Bianchi, L. (1994). Posterior parietal cortex: Functional properties of neurons in area 5 during an instructed-delay reaching task within different parts of space. *Experimental Brain Research, 99,* 175–178.

Flash, T., & Mussa-Ivaldi, F. (1990). Human arm stiffness characteristics during the maintenance of posture. *Experimental Brain Research, 82,* 315–326.

Gail, A., Klaes, C., & Westendorff, S. (2009). Implementation of spatial transformation rules for goal-directed reaching via gain modulation in monkey parietal and premotor cortex. *Journal of Neuroscience, 29,* 9490–9499.

Galletti, C., Fattori, P., Kutz, D. F., & Gamberini, M. (1999). Brain location and visual topography of cortical area V6A in the macaque monkey. *European Journal of Neuroscience, 13,* 1572–1588.

Gamberini, M., Passarelli, L., Fattori, P., Zucchelli, M., Bakola, S., Luppino, G., et al. (2009). Cortical connections of the visuomotor parietooccipital area V6Ad of the macaque monkey. *Journal of Comparative Neurology, 513,* 622–642.

Gauthier, G. M., & Mussa-Ivaldi, F. (1988). Oculo-manual tracking of visual targets in monkey: Role of the arm

afferent information in the control of arm and eye movements. *Experimental Brain Research, 73,* 138–154.
Georgopoulos, A. P. (2000). Neural aspects of cognitive motor control. *Current Opinion in Neurobiology, 10,* 238–241.
Georgopoulos, A. P., Kalaska, J. F., Caminiti, R., & Massey, J. T. (1982). On the relations between the direction of two-dimensional arm movements and cell discharge in primate motor cortex. *Journal of Neuroscience, 2,* 1527–1537.
Ghilardi, M. F., Alberoni, M., Marelli, S., Rossi, M., Franceschi, M., Ghez, C., et al. (1999). Impaired movement control in Alzheimer's disease. *Neuroscience Letters, 260,* 45–48.
Gielen, C. C., Van Den Heuvel, P. J., & Van Gisbergen, J. A. (1984). Coordination of fast eye and arm movements in a tracking task. *Experimental Brain Research, 56,* 154–161.
Gorbet, D. J., & Sergio, L. E. (2007). Sex-related differences in cortical activity during visually-guided movements. *European Journal of Neuroscience, 25,* 1228–1239.
Gorbet, D. J., & Sergio, L. E. (2009). The behavioral consequences of dissociating the spatial directions of eye and arm movements. *Brain Research, 1284,* 77–88.
Gorbet, D. J., Staines, W. R., & Sergio, L. E. (2004). Brain mechanisms for preparing increasingly complex sensory to motor transformations. *Neuroimage, 23,* 1100–1111.
Henriques, D. Y. P., Klier, E. M., Smith, M. A., Lowy, D., & Crawford, J. D. (1998). Gaze-centered remapping of remembered visual space in an open-loop pointing task. *Journal of Neuroscience, 18,* 1583–1594.
Jacobs, H. I. L., Van Boxtel, M. P. J., Uylings, H. B. M., Gronenschild, E. H. B. M., Verhey, F. R., & Jolles, J. (2010). Atrophy of the parietal lobe in preclinical dementia. *Brain and Cognition, 75,* 154–163.
Johnson, P. B., Ferraina, S., Bianchi, L., & Caminiti, R. (1996). Cortical networks for visual reaching: Physiological and anatomical organization of frontal and parietal lobe arm regions. *Cerebral Cortex, 6,* 102–119.
Kalaska, J. F. (1996). Parietal cortex area 5 and visuomotor behavior. *Canadian Journal of Physiology and Pharmacology, 74,* 483–498.
Kalaska, J. F., Cohen, D. A., Hyde, M. L., & Prud'homme, M. (1989). A comparison of movement direction-related versus load direction-related activity in primate motor cortex, using a two-dimensional reaching task. *Journal of Neuroscience, 9,* 2080–2102.
Kalaska, J. F., & Crammond, D. J. (1995). Deciding not to go: Neuronal correlates of response selection in a go/nogo task in primate premotor and parietal cortex. *Cerebral Cortex, 5,* 410–428.
Kalaska, J. F., Sergio, L. E., & Cisek, P. (1998). Cortical control of whole-arm motor tasks. *Novartis Foundation Symposium, 218,* 176–190.
MacKay, W. A., & Crammond, D. J. (1987). Neuronal correlates in posterior parietal lobe of the expectation of events. *Behavioural Brain Research, 24,* 167–179.
Marzocchi, N., Breveglieri, R., Galletti, C., & Fattori, P. (2008). Reaching activity in parietal area V6A of macaque: Eye influence on arm activity or retinocentric coding of reaching movements? *European Journal of Neuroscience, 27,* 775–789.
Medendorp, P. W., Goltz, H. C., Crawford, J. D., & Vilis, T. (2005). Integration of target and effector information in human posterior parietal cortex for the planning of action. *Journal of Neurophysiology, 93,* 954–962.
Morasso, P. (1981). Spatial control of arm movements. *Experimental Brain Research, 42,* 223–227.
Neggers, S. F. W., & Bekkering, H. (2000). Ocular gaze is anchored to the target of an ongoing pointing movement. *Journal of Neurophysiology, 83,* 639–651.
Piaget, J. (1965). *The construction of reality in the child*. New York: Basic Books, Inc.
Prablanc, C., Echallier, J. F., Komilis, E., & Jeannerod, M. (1979). Optimal response of eye and hand motor systems in pointing at a visual target. I. Spatio-temporal characteristics of eye and hand movements and their relationships when varying the amount of visual information. *Biological Cybernetics, 35,* 113–124.
Prado, J., Clavagnier, S., Otzenberger, H., Scheiber, C., Kennedy, H., & Perenin, M. (2005). Two cortical systems for reaching in central and peripheral vision. *Neuron, 48,* 849–858.
Redding, G. M., Rossetti, Y., & Wallace, B. (2005). Applications of prism adaptation: A tutorial in theory and method. *Neuroscience and Biobehavioral Reviews, 29,* 431–444.
Redding, G. M., & Wallace, B. (1996). Adaptive spatial alignment and strategic perceptual-motor control. *Journal of Experimental Psychology: Human Perception and Performance, 22,* 379–394.
Salek, Y., Anderson, M. D., & Sergio, L. E. (2011). Mild cognitive impairment is associated with impaired visual-motor planning when visual stimuli and actions are incongruent. *European Neurology, 66,* 283–293.
Schroeter, M. L., Stein, T., Maslowski, N., & Neumann, J. (2009). Neural correlates of Alzheimer's disease and mild cognitive impairment: A systematic and quantitative meta-analysis involving 1351 patients. *Neuroimage, 47,* 1196–1206.
Seal, J., Gross, C., & Bioulac, B. (1982). Activity of neurons in area 5 during a simple arm movement in monkeys before and after deafferentation of the trained limb. *Brain Research, 250,* 229–243.
Seal, J., Gross, C., Doudet, D., & Bioulac, B. (1983). Instruction-related changes of neuronal activity in area 5 during a simple forearm movement in the monkey. *Neuroscience Letters, 36,* 145–150.
Sergio, L. E., Gorbet, D. G., Tippett, W. J., Yan, X., & Neagu, B. (2009). When what you see isn't where you get: Cortical mechanisms of vision for complex action. In M. Jenkin & L. Harris (Eds.), *Cortical mechanisms of vision* (pp. 81–111). New York: Cambridge University Press.
Sergio, L. E., & Kalaska, J. F. (2003). Systematic changes in motor cortex cell activity with arm posture during directional isometric force generation. *Journal of Neurophysiology, 89,* 212–228.
Sergio, L. S., & Scott, S. H. (1998). Hand and joint paths during reaching movements with and without vision. *Experimental Brain Research, 122,* 57–164.
Shen, L., & Alexander, G. E. (1997). Preferential representation of instructed target location versus limb trajectory in dorsal premotor area. *Journal of Neurophysiology, 77,* 1195–1212.
Stoet, G., & Snyder, L. (2004). Single neurons in posterior parietal cortex of monkeys encode cognitive set. *Neuron, 42,* 1003–1012.
Tippett, W. J., Krajewski, A., & Sergio, L. E. (2007). Visuomotor integration is compromised in Alzheimer's disease patients reaching for remembered targets. *European Neurology, 58,* 1–11.

Tippett, W. J., & Sergio, L. E. (2006). Visuomotor integration is impaired in early stage Alzheimer's disease. *Brain Research, 1102,* 92–102.
Vercher, J. L., Magenes, G., Prablanc, C., & Gauthier, G. M. (1994). Eye-head-hand coordination in pointing at visual targets: Spatial and temporal analysis. *Experimental Brain Research, 99,* 507–523.
Weinrich, M., Wise, S. P., & Mauritz, K. H. (1984). A neurophysiological study of the premotor cortex in the rhesus monkey. *Brain, 107,* 385–414.
White, I. M., & Wise, S. P. (1999). Rule-dependent neuronal activity in the prefrontal cortex. *Experimental Brain Research, 126,* 315–335.
Wise, S. P., di Pellegrino, G., & Boussaoud, D. (1996). The premotor cortex and nonstandard sensorimotor mapping. *Canadian Journal of Physiology and Pharmacology, 74,* 469–482.
Zhang, J., Riehle, A., Requin, J., & Kornblum, S. (1997). Dynamics of single neuron activity in monkey primary motor cortex related to sensorimotor transformation. *Journal of Neuroscience, 17,* 2227–2246.